

## Total electron yield of layered synthetic materials with interfacial roughness

A. Krol, C. J. Sher, and Y. H. Kao

*Department of Physics, State University of New York at Buffalo, Buffalo, New York 14260*

(Received 11 April 1990)

The applicability of grazing-angle total-electron-yield spectroscopy as a tool for probing the microstructures in layered synthetic materials is investigated. A model proposed for describing the angular variation of grazing-incidence total electron yield (TEY) is shown to agree well with experimental results. Both theoretical and experimental evidence indicates that the probing depth in this angular TEY spectroscopy for layered structures is comparable with the characteristic x-ray attenuation length and is not limited by the inelastic mean free path of secondary electrons that dominate the TEY signal. This technique can therefore be used as a convenient tool for in-depth microstructural studies of various layered materials.

### I. INTRODUCTION

Excitation of photoelectrons by x ray gives rise to the creation of core holes which may decay either in radiative or nonradiative transitions. Products of these processes can be detected by means of x-ray fluorescence or electron yield. The energy spectrum of the emitted electrons usually consists of well-defined lines due to photoelectrons and Auger electrons on top of a background due to secondary electrons. These low-energy secondary electrons, resulting from inelastic collisions of initially excited photoelectrons and Auger electrons, give rise to a major portion of the electron emission, and the sample can be regarded as an effective electron multiplier. Monitoring the total electron yield (TEY), i.e., all electrons emitted from the sample, offers the simplest mode for detecting the photoabsorption process. TEY measurements have been employed in (surface) extended x-ray-absorption fine-structure [(S)EXAFS] investigations for the determination of the local order near the surface<sup>1-3</sup> and in the bulk of solids.<sup>4-9</sup> They have also been carried out to study x-ray standing waves, lattice distortions, and other parameters in crystals.<sup>10-13</sup> Recently a considerable effort has been undertaken in order to construct a quantitative model of x-ray-induced TEY from solids in the context of EXAFS experiments.<sup>14-18</sup> The x-ray-excited secondary electron emission from metals, semiconductors, and insulators was studied theoretically and experimentally by Henke *et al.*<sup>19,20</sup> In this pioneering work a model was developed which provided a satisfactory explanation of the experimental data.

In the present paper we discuss the applicability of TEY method to the investigation of microstructures in layered synthetic materials (LSM). We demonstrate that, by monitoring the x-ray-induced TEY versus grazing-incidence angle at a fixed incoming photon energy, one can obtain information on the microstructures not only in the near-surface region but also about the buried interfaces, in spite of a very short inelastic mean free path (IMFP) of secondary electrons. This interesting result is a consequence of the fact that electron emission from stratified medium is determined by the radiant energy

losses in the near-surface region, which is the primary source of total electron yield, and this process is governed by the electromagnetic field distribution in the entire stratified medium. Even distant boundaries (interfaces), as compared with secondary-electron IMFP, can strongly influence the angular TEY profile.

In a previous publication<sup>21</sup> radiant energy flow in a finite multilayer system with rough interfaces was analyzed. The optical electromagnetic wave solution of the Fresnel equation (OEMF) on each interface together with a vector theory<sup>22</sup> for specularly scattered radiation was used. This model was then employed for the analysis of experimental x-ray fluorescence yield data with satisfactory agreement. We now apply this model to the problem of TEY from stratified media and demonstrate that the TEY technique can be used for probing the microstructures in layered synthetic materials. We would like to note that detection of TEY is especially attractive in a soft x-ray region or for low-Z materials in view of the extremely small fluorescence yield in these cases.<sup>23</sup>

### II. TOTAL ELECTRON YIELD FROM LSM WITH ROUGH INTERFACES

#### A. General description of the model

As we mentioned before, secondary electrons dominate the x-ray-generated total electron yield and the contribution of primary electrons to this process can be neglected in the first approximation.<sup>15-20</sup> For this reason, in the due course of this paper, we shall focus our attention on the problem of secondary-electron emission from stratified media. In order to describe the x-ray-generated secondary-electron emission from solids one has to consider the following steps.

- (1) Excitation of primary electrons.
- (2) Creation of secondary electrons.
- (3) Migration of secondary electrons to the surface.
- (4) Escape into vacuum.

This kind of approach to photoelectron emission from

solids is known as the three-step model (i.e., creation, diffusion, and escape of photoelectrons into vacuum).<sup>24</sup> The basic idea of this concept is that the complex photoemission process can be decomposed into independent (in the first approximation) steps.

### B. Excitation of primary electrons

The first step can be realized only if the energy of the incoming x-ray photons exceeds a characteristic excitation threshold for a given core level. As a result, a single hole and a single photoelectron are created. This hole can be filled radiatively with the emission of a fluorescence photon, or nonradiatively via the Auger process. A consequence of the fluorescence emission is that a single hole is created in a higher shell. The Auger process gives rise to the creation of two holes in higher orbitals. Self-photoabsorption of some of the primary fluorescence photons results in the creation of secondary core vacancies. The secondary holes decay through either the radiative or nonradiative channel, although the probability of radiative recombination usually becomes smaller for higher shells.<sup>25</sup> Thus, any absorbed x-ray photon may give rise to a number of photoelectrons and Auger electrons.<sup>18</sup> The radiant energy dissipation of incoming x-ray radiation can be modeled by means of the above-mentioned OEMF theory<sup>21</sup> and is a function of the grazing-incidence angle, energy of incoming x-ray photons, boundary conditions, and material constants of the layered structure. The flux loss in the infinitesimal layer with thickness  $dz$ , at depth  $z$  for the energy of incoming radiation  $E_0$  can be described by the function  $L(E_0, \theta, z)$ :

$$L(E_0, \theta, z) = - \frac{dF(E_0, \theta, z)}{dz}, \quad (1)$$

where  $\theta$  is the grazing angle of incidence and  $F(E_0, \theta, z)$  is the radiant flux.<sup>21</sup>

The density of photoelectron production, i.e., the number of primary photoelectrons of  $q$  type emitted into solid angle  $d\omega$ , in the direction  $y$ , per unit time, from a small volume  $dV$ , at the depth  $z$  is proportional to the radiant energy lost in this volume, viz.,

$$\left[ \frac{d^3 N_q}{dt dV d\omega} \right]_y = F_0 c_q(z) [d\sigma_q(E_0)/d\omega]_y L(E_0, \theta, z) = P_{qy}(E_0, \theta, z), \quad (2)$$

where  $F_0$  is the incoming flux and  $c_q(z)$  is the concentration of atoms which emit the  $q$ -type photoelectrons.  $[d\sigma_q(E_0)/d\omega]_y$  is the differential partial photoionization cross section which is a function of the initial electron state  $q$  and exhibits strong anisotropy.<sup>26</sup>

The density of primary Auger-electron creation due to  $qrs$ -type Auger transitions at the depth  $z$  is

$$\frac{d^3 N_{qrs}}{dt dV d\omega} = F_0 c_q(z) [\sigma_q(E_0)/4\pi] a_{qrs} L(E_0, \theta, z) = A_{qrs}(E_0, \theta, z), \quad (3)$$

where  $a_{qrs}$  is the probability of  $qrs$ -type Auger process,<sup>25</sup>

$\sigma_q(E_0)$  is the angle-integrated partial photoionization cross section since the angular distribution of Auger-electron emission is isotropic.

### C. Creation of secondary electrons

Let us consider now step (2), i.e., secondary-electron generation. The excited primary electrons in solids are scattered either elastically (via a screened Rutherford cross section, with large scattering angles) or inelastically (with small scattering angles).<sup>27–29</sup> Inelastic scattering results from collisions with the conduction-, valence-, and inner-atomic-shell electrons, bulk and surface or interfacial plasmons, phonons, and other excitations. There are many theoretical treatments of inelastic scattering of electrons in solids. The Born-Bethe theory<sup>30</sup> or continuous slowing-down approximation is based on the fact that, in the majority of inelastic collisions, the energy is dissipated in relatively small steps (of the order of a few to tens of eV). However, larger energy losses due to core-level excitations result in “straggling” of the penetration ranges and lead to some discrepancies with experiment. This problem was treated by Sugiyama<sup>31</sup> who corrected the theory for inner-shell excitations. In the statistical model, sometimes called the “optical” approximation,<sup>27,32–34</sup> the inelastic mean free path is calculated from the dielectric response function. A Monte Carlo approach was also successfully applied to the direct simulation of energy dissipation by the excited electrons in solids.<sup>27</sup> One can distinguish different classes of secondary electrons excited by x-ray radiation<sup>19,20</sup> as follows.

- (i) Direct secondaries created by fast primaries which, at early stages of their transport through the solid, can only interact weakly with conduction or valence electrons and the energy transfer is very limited.
- (ii) Direct secondaries due to inelastic scattering of slowed-down (below 100 eV) primaries.
- (iii) Indirect secondaries created in cascade process of direct secondaries.
- (iv) Indirect secondaries generated via plasmon decay.

Henke *et al.*<sup>19,20</sup> have defined the conversion efficiency factor  $f(E_0)$  describing the total number of secondary electrons created per unit energy of the x-ray photons with energy  $E_0$ . They have shown that this factor only depends weakly on the photon energy except for some small discontinuities at x-ray-absorption edges. They have also proved that the energy distribution of secondary electrons does not depend on the primary-electron energy or the incident photon energy. This means that the direct and indirect processes of the secondaries production have a similar energy dependence. Their results have been confirmed recently by Matthew *et al.*<sup>35</sup> who observed a similar power-law form of the secondary-electron-energy distribution.

Our model is based on the following assumptions.

- (i) The number of the direct secondary electrons created per unit distance along the path of the primary electrons is proportional to the average energy loss divided by the average energy of secondaries.

(ii) The indirect secondary electrons are generated in the vicinity (i.e., within the range comparable to their IMFP) of the paths of the primaries and the density of their generation is also proportional to the energy loss of primaries along their trajectories divided by the average energy of secondaries.

(iii) Due to the randomizing nature of their creation, the secondaries have isotropic velocity distribution.

Historically the above description of the secondary-electron generation, although without distinguishing between direct and indirect secondaries, was first introduced by Bruining<sup>36</sup> and Salow.<sup>37</sup> Henke *et al.*,<sup>19,20</sup> following the calculation of Stoltz,<sup>38</sup> have proven theoretically and experimentally that assumption (ii) holds in the so-called isotropic approximation. Cargill *et al.*<sup>17,18</sup> proposed a model with a basic assumption that all secondary electrons are homogeneously generated within the penetration range of the primaries and the total number of created secondaries is equal to the energy of primary electrons divided by the average energy of secondaries. In their model they did not distinguish between the direct and indirect secondaries. Despite its simplicity, this model describes reasonably well the observed edge jumps versus overlayer thickness as measured by means of TEY in the hard x-ray regime.

The contribution to the secondary-electron generation at point  $\mathbf{r}$  due to the creation of  $q$ -type photoelectrons at the point  $\mathbf{r}_0$  is given by

$$n_q(\mathbf{r}, \mathbf{r}_0) = P_{qv}(E, \theta, \mathbf{r}_0) S_q(\mathbf{r}) / \varepsilon, \quad (4)$$

where  $S_q(\mathbf{r})$  is the stopping power of the medium at point  $\mathbf{r}$  experienced by a  $q$  photoelectron along its trajectory,  $P_{qv}(E, \theta, \mathbf{r}_0)$  is given by (2), and  $\varepsilon$  is the average energy of the secondaries in the solid.

The contribution to the secondary-electron generation at point  $\mathbf{r}$  due to the creation of a  $qrs$ -type Auger electron at point  $\mathbf{r}_0$  is

$$n_{qrs}(\mathbf{r}, \mathbf{r}_0) = A_{qrs}(E, \theta, \mathbf{r}_0) S_q(\mathbf{r}) / \varepsilon, \quad (5)$$

where  $A_{qrs}(E, \theta, \mathbf{r}_0)$  is given by (3).

#### D. Diffusion of secondary electrons

In the present proposed model the probability  $P_\varepsilon(z)$  of secondary electrons created at a depth  $z$  to reach just below the surface is given by the exponential absorption law<sup>19,20,39,40</sup> with the appropriate attenuation length equal to the IMFP for the secondaries with the average energy  $\varepsilon$ . We have

$$P_\varepsilon(z) = \frac{1}{2} \int_0^{\pi/2} \exp\left[-\frac{z}{l_\varepsilon \cos y}\right] \sin y \, dy, \quad (6)$$

where  $l_\varepsilon$  is the mean free path of the secondary electrons with average energy  $\varepsilon$  and  $y$  is the polar emission angle measured from the direction normal to the interfaces.

#### E. Emission of secondary electrons into vacuum

In step (4) we consider the secondary electrons escape into vacuum through the surface potential barrier. This

process is described by the threshold function  $T(E)$ , which is a smooth function of kinetic energy of the secondaries.<sup>15,19,20,40</sup> The existence of the surface barrier results in drastic attenuation of the secondary-electron-energy distribution at very low energies.

#### F. Total-electron-yield intensity

In the framework of our model the total electron yield [denoted by  $i_{\text{TEY}}(\theta)$ ] from a layered structure mainly consists of secondary electrons generated by primary photoelectrons and Auger electrons, denoted by  $i_q(\theta)$  and  $i_{qrs}(\theta)$ , respectively,

$$i_{\text{TEY}}(\theta) = \sum_q \left[ i_q(\theta) + \sum_{r,s} i_{qrs}(\theta) \right], \quad (7)$$

where the summation is over all accessible states  $qrs$ . The first component may be written as

$$i_q(\theta) = CT(\varepsilon) \int_S \int_S P_\varepsilon(z) n_q(\mathbf{r}, \mathbf{r}_0) d^3r d^3r_0, \quad (8)$$

where the double integral is evaluated over the stratified medium down to a depth comparable with the x-ray attenuation length and  $C$  is a constant. The second component is

$$i_{qrs}(\theta) = CT(\varepsilon) \int_S \int_S P_\varepsilon(z) n_{qrs}(\mathbf{r}, \mathbf{r}_0) d^3r d^3r_0. \quad (9)$$

### III. PREDICTIONS OF THE MODEL

Quantitative estimation of the energy dissipation by the primary electrons in solids is hindered at low energies (below 200 eV) due to the lack of a reliable theory (see discussion by Tung *et al.*<sup>32</sup> and Penn<sup>34</sup>). For this reason we decided to use the Born-Bethe slowing-down approximation in a form proposed by Sugiyama<sup>31</sup> for its simplicity. This treatment includes inner-shell and plasmon corrections and offers a simple phenomenological description. In this approach two parameters are introduced: the effective mean excitation energy  $J^*(E)$  and the effective number of electrons per scattering atoms  $Z^*(E)$ . Both parameters are a function of the energy of the slowing-down electron. A plasmon loss correction is taken into account in the form proposed by Quinn.<sup>41</sup> Unfortunately, at low primary energies one expects some discrepancies of this theory with experiment. However, we do believe that this fact does not change the conclusions significantly. This is supported by our model studies of the influence of the shape of the primary-electron-energy-loss function on TEY and no substantial changes in the predicted TEY angular profile were found. In Sec. IV it is discussed that various TEY models show little dependence on the shape of the primary-electron-energy-loss function.

Due to the existence of an axial symmetry in the layered structure, the energy losses are a function of the polar angle (with reference to the axis of symmetry). We illustrate this by example of a (Pt/C)  $\times$  30/C superlattice which consists of 30 double layers of C and Pt with 14.4- and 17.3-Å thickness, respectively, on a carbon substrate. The stopping power calculated for the direction parallel to the boundaries (in the Pt layer) of the stratified medium is shown in Fig. 1 for a number of different initial en-

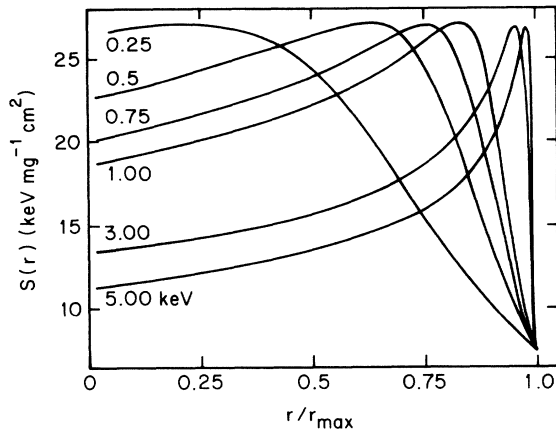


FIG. 1. Stopping power  $S(r)$  in a  $[\text{Pt}(17.3 \text{ \AA})/\text{C}(14.4 \text{ \AA})] \times 30/\text{C}$  superlattice (30 double layers of C and Pt with 14.4- and 18- $\text{\AA}$  thickness, respectively, on a carbon substrate) vs reduced distance from the point of emission for primary electron in the direction parallel to the boundaries. Point of emission is assumed to be in a Pt layer.  $r_{\text{max}}$  denotes the penetration range for electrons with a given initial energy.

ergies of the primary electrons. As we see, the higher is the initial energy the more energy is dissipated farther from the origin. The primary electron with 0.25-keV initial energy loses a majority of its energy within a distance smaller than half of its penetration range while an electron with 5-keV initial energy does it in the distance larger than 75% of its range. This is also true for other directions, as illustrated in Fig. 2, for the direction normal to the interfaces of the LSM. Another striking feature predicted by the Born-Bethe theory is the jumps of the stopping power at the boundaries. Before we discuss the density of secondary-electron production distribution in the LSM, given by (4), let us consider the creation of secondaries via the excitation of photoelectrons. Due to the strong angular anisotropy of the photoelectron emission<sup>26</sup> mentioned above, one can expect a characteristic distribution pattern which lacks spherical symmetry as shown in Fig. 3 which exhibits "islands" of high-density secondary-electron production. The results of application of (4) to the  $(\text{Pt}/\text{C}) \times 30/\text{C}$  superlattice are shown in Fig. 4. The presence of the LSM boundaries results in jumps and discontinuities of the isodensity contours as compared with bulk Pt. The "island" of the maximum density of secondary-electron production are, in this case, topologically limited by the layer size.

The production of the secondaries due to dissipation of energy by the primary Auger electrons is expected to be spherically symmetric in a homogeneous medium as shown in Fig. 5 for bulk Pt, calculated by using (5). This symmetry is not observed in the superlattice. As expected, the presence of the boundaries imposes discontinuities in the isodensity contours, illustrated in Fig. 6 for the  $(\text{Pt}/\text{C}) \times 30/\text{C}$  superlattice.

A simple case of a stratified medium is represented by a heterostructure. For this reason we will first consider the prediction of the present model as applied to x-ray-generated secondary electron emission from a thin (as compared with the x-ray attenuation length) overlayer on

a substrate. As an example, we will consider the GaAs/AlAs heterostructure. In order to calculate the TEY current from this system [Eq. (7)] one has to evaluate the average energy of the secondary electrons and the corresponding attenuation length. The average kinetic energy of the emitted secondaries excited by x-ray photons with energies in the range 0.1–10 keV is of the order of 2 eV.<sup>19,20</sup> The average secondary-electron energy inside the solid can be estimated based on the assumed excitation function<sup>20,42</sup> and the work function. As a result, one obtains a value between 5 and 10 eV for most solids. Using published data<sup>32,34,43–48</sup> for the IMFP of low-energy electrons in solids, one can estimate the corresponding attenuation length of the "average" secondaries as being in the range 20–60  $\text{\AA}$ . One can now calculate the TEY current components from (8) and (9). The results of the calculation for a GaAs/AlAs heterostructure

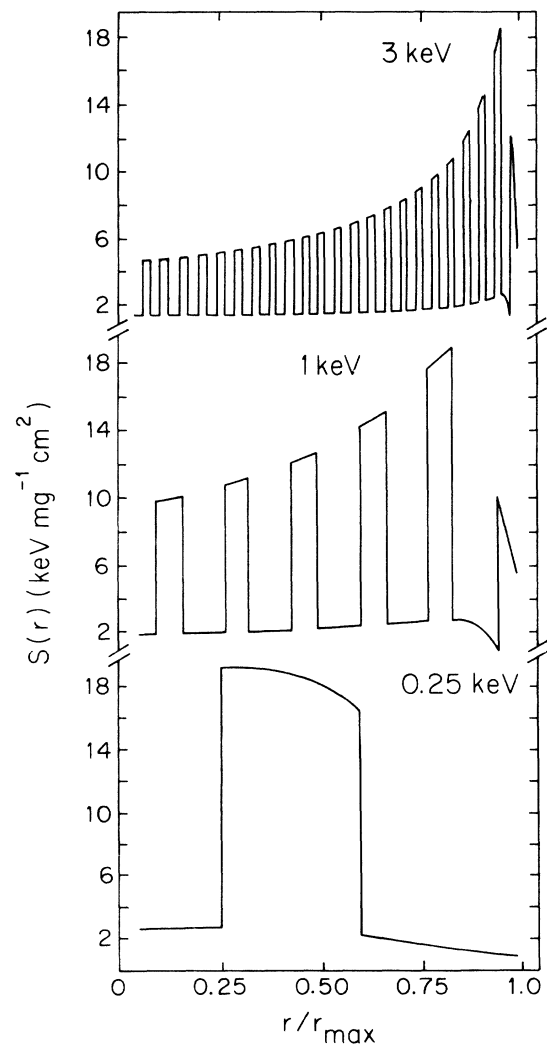


FIG. 2. Stopping power  $S(r)$  in a  $[\text{Pt}(17.3 \text{ \AA})/\text{C}(14.4 \text{ \AA})] \times 30/\text{C}$  superlattice vs reduced distance from the point of emission of primary electron in the direction perpendicular to the boundaries. Point of emission is assumed to be in a Pt layer.

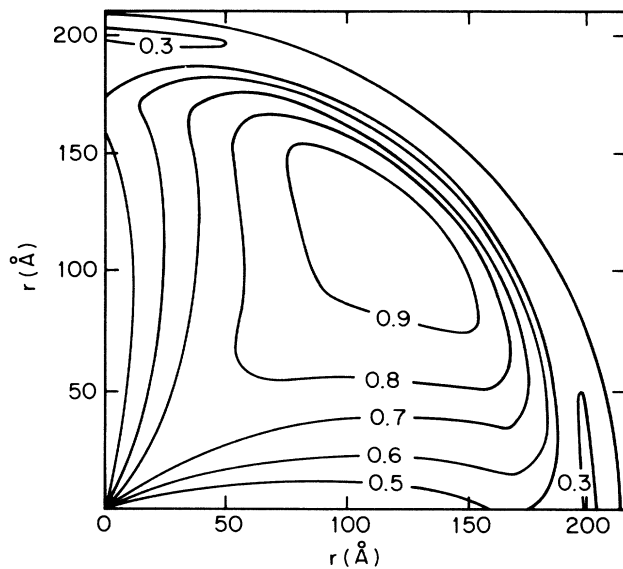


FIG. 3. Plots of isodensity of the secondary-electron production contours in a bulk solid platinum due to photoelectrons excited at the origin with energy  $E_q = 0.93$  keV. The incidence angle is selected at  $\pi/4$  rad and the radiation is polarized in the plane perpendicular to the plane of incidence (TE case). The ordinate axis is parallel to the surface.

with different overlayer thickness are shown in Fig. 7. A very significant feature of these TEY angular profiles is the presence of well-defined interference oscillations at grazing-incidence angles higher than the critical-incidence angle. This interference pattern stems from the

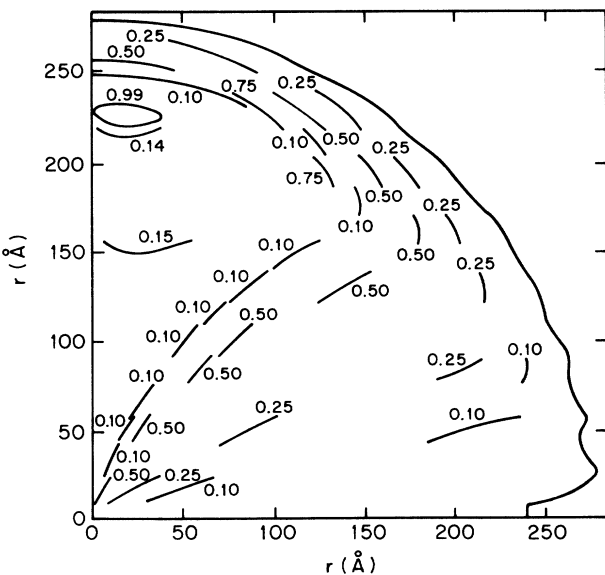


FIG. 4. Plots of isodensity of the secondary-electron production contours in a  $[\text{Pt}(17.3 \text{ \AA})/\text{C}(14.4 \text{ \AA})] \times 30/\text{C}$  superlattice due to photoelectrons excited at the origin (in the middle of a Pt layer) with energy  $E_q = 0.93$  keV. The incidence angle is selected at  $0.087$  rad and the radiation is polarized in the plane perpendicular to the plane of incidence (TE case). The ordinate axis is parallel to the interfaces.

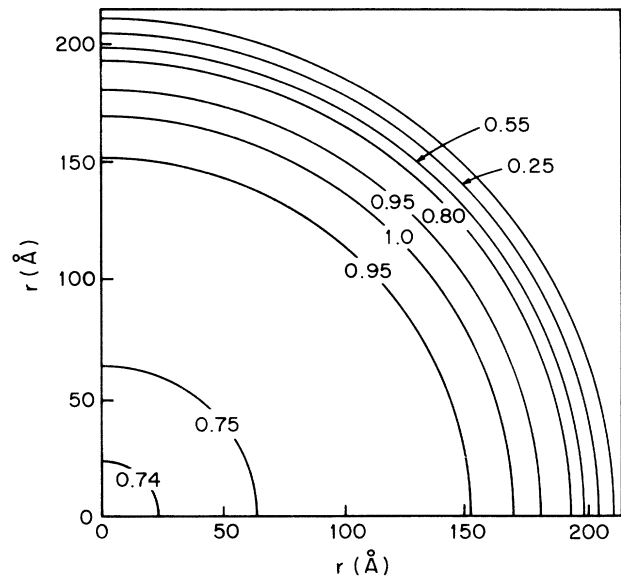


FIG. 5. Plots of isodensity of the secondary-electron production contours in a bulk solid platinum due to Auger electrons excited at the origin with energy  $E_{grs} = 0.93$  keV. The ordinate axis is parallel to the surface.

existence of the buried interface. The period and the amplitude of oscillations is inversely proportional to the overlayer thickness. In Fig. 8 the influence of roughness on the TEY angular profile is shown. Our TEY model predicts that the oscillation amplitude is an inverse function of the interfacial roughness. The surface roughness strongly influences the evanescence region of the TEY profiles, and increases and broadens the TEY curve around the critical angle.

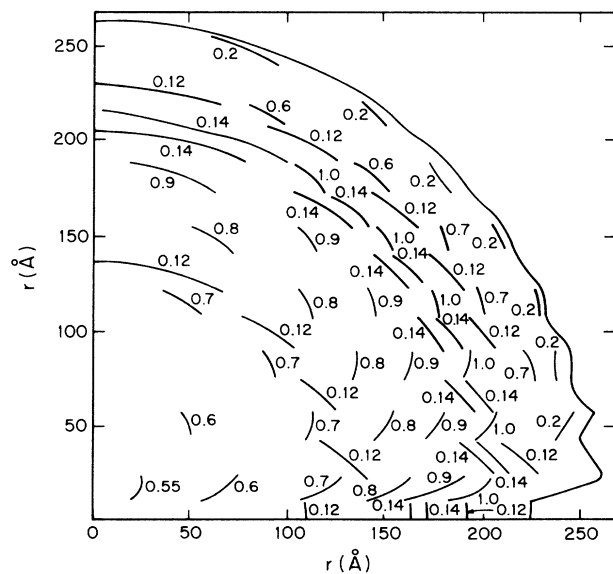


FIG. 6. Plot of isodensity of the secondary-electron production contours in a  $[\text{Pt}(17.3 \text{ \AA})/\text{C}(14.4 \text{ \AA})] \times 30/\text{C}$  superlattice due to Auger electrons excited at the origin (in the middle of a Pt layer) with energy  $E_{grs} = 0.93$  keV. The ordinate axis is parallel to the interfaces.

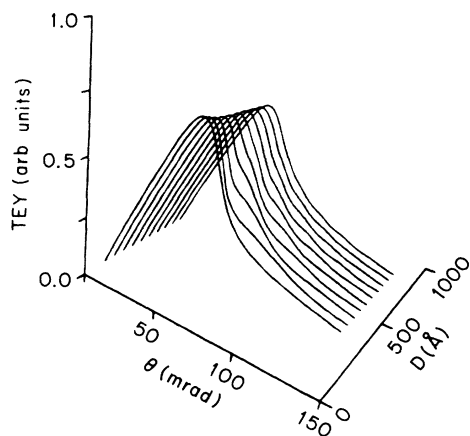


FIG. 7. Influence of the overlayer thickness on TEY from a GaAs/AlAs heterostructure. The energy of the x ray is 600 eV.  $D$  is the overlayer thickness. The surface and interface are assumed to be ideal smooth planes.

In Fig. 9 an angular TEY profile is shown, calculated for the (PT/C) $\times$ 30/C superlattice at the energy of an x ray equal to 930 eV. For comparison, the total radiant energy dissipated in all carbon and platinum layers versus incidence angle is also shown [Figs. 9(a) and 9(c), respectively]. Because, in this case, the majority of all primary

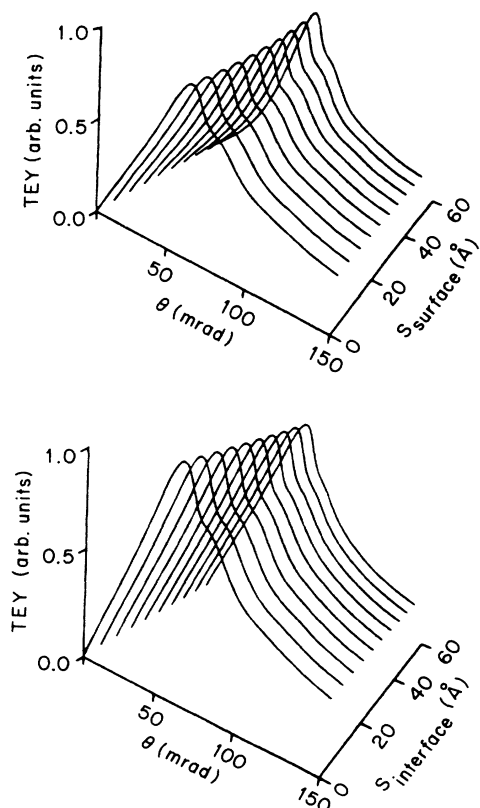


FIG. 8. Influence of surface and interfacial roughness on TEY from a GaAs/AlAs heterostructure with a 250-Å overlayer thickness. The energy of the x ray is 600 eV.  $S$  is a roughness parameter, representing the rms deviation from an ideal smooth plane interface.

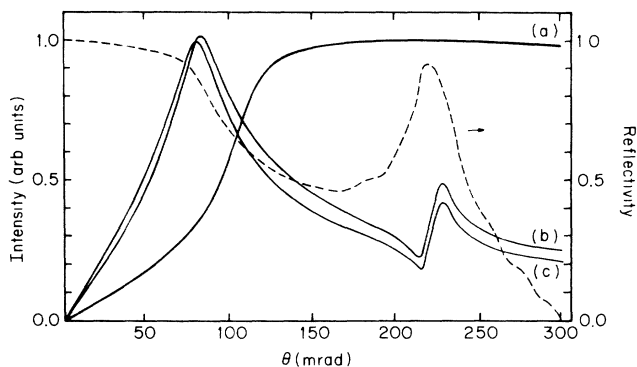


FIG. 9. (a) The total radiant energy dissipated in all carbon layers vs grazing angle of incidence in a [Pt(17.3 Å)/C(14.4 Å)] $\times$ 30/C superlattice for 5-keV energy of incoming photons, (b) TEY from this superlattice, (c) the total radiant energy dissipated in all platinum layers vs grazing angle of incidence in this superlattice. The corresponding x-ray reflectivity is shown by the dashed line. The energy of the x ray is 930 eV. The surface and all interfaces are assumed to be ideal smooth planes.

electrons are created in Pt layers, the TEY curve [Fig. 9(b)] resembles the radiant energy-loss curve integrated over all Pt layers. Another important feature is the presence of the first Bragg reflection peak at 0.222 rad. As we see, the TEY curve exhibits a characteristic minimum at this angle due to the presence of nodal planes of the Poynting vector in the Pt layers. At slightly higher angles the antinodal planes are in the Pt layers and one expects a maximum in the radiant energy dissipated in these strata ergo maxima in the TEY.

The influence of roughness on the TEY angular profile for a superlattice is shown in Fig. 10. As expected, the surface roughness influences mainly the evanescent region of the curve, in the form of broadening and increasing the TEY maximum. Increasing the interfacial roughness results in blurring the Bragg-related TEY maximum of the multilayer (around 222 mrad) which vanishes when

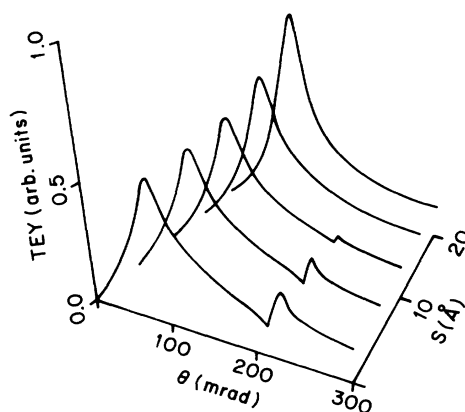


FIG. 10. Influence of surface and interfacial roughness on TEY from a [Pt(17.3 Å)/C(14.4 Å)] $\times$ 30/C superlattice. The energy of the x ray is 930 eV.  $S$  is a roughness parameter, representing the rms deviation from an ideal smooth plane interface.

the rms roughness parameter becomes comparable to the layer thickness.

#### IV. COMPARISON WITH OTHER MODELS

In Fig. 11 predictions based on different models of TEY are shown. Calculations were performed for bulk Pt for energy of incoming photons equal to 5 keV. The solid line represents the results obtained in the framework of the TEY model proposed by Cargill *et al.*<sup>17,18</sup> Their model assumes that the secondary electrons are created uniformly within spheres with radii equal to the penetration ranges of primary electrons and anisotropy of the emission of primaries is neglected. The next lower curve was obtained by assuming that the secondary electrons are created with intensity proportional to the stopping power of the solid but the angular distribution of the primary-electron emission is isotropic. We would like to note that even though the high-energy primaries deposit a majority of energy in the last quarter of their traversed paths (see Fig. 1) and the distribution of the secondary sources is drastically different from that in the homogeneous model by Cargill *et al.*,<sup>17,18</sup> the general shape of the TEY angular profile does not change and the TEY current is merely lowered by a few percent. This is due to the fact that the IMFP of the secondaries is much smaller than the x-ray attenuation length.

The third curve from the top was obtained assuming proper angular distribution of the emitted primary photoelectrons and homogeneous creation of secondary electrons within the penetration ranges of primaries. This as-

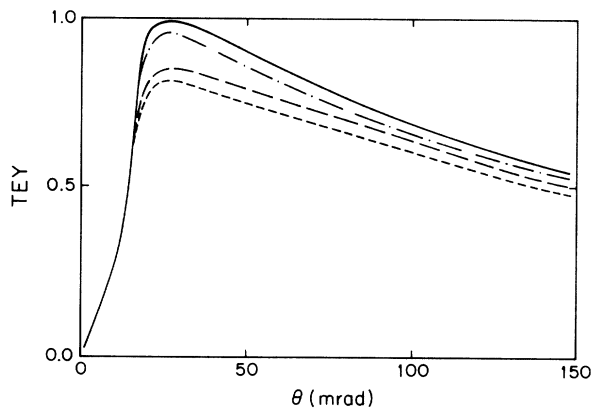


FIG. 11. Predictions of TEY based on different models. Calculations were performed for bulk Pt for the energy of incoming photons equal to 5 keV. The solid lines represents the results obtained in the framework of the TEY model proposed by Cargill *et al.* (Refs. 17 and 18). The dot-dashed curve was obtained by assuming that the secondary electrons are created with an intensity proportional to the stopping power of the solid, but the angular distribution of the primary-electron emission is isotropic. The long-dashed line was obtained assuming proper angular emission of the primary photoelectrons and homogeneous creation of secondary electrons within the penetration ranges of primaries. The short-dashed line was obtained in the framework of the model proposed here.

sumption results in a broadening of the TEY curve and further reduction of the TEY intensity (by 18% in the maximum) as compared to the uniform emission model. The lowest TEY angular profile was obtained in the framework of the model proposed here. The TEY curve has the same shape as in the previously discussed model but the intensity is further reduced (by 23% at the maximum).

In summary, the shape of the TEY angular profile is influenced by the angular distribution of the primary-electron emission but practically not by the density of the emission-source distribution. In many practical cases, especially for energies just above the absorption edges where a majority of secondaries is created by Auger electrons, all the models give virtually identical results and the model of Cargill *et al.*<sup>17,18</sup> with analytical formulas can be used to avoid tedious numerical integrations. However, far away from the absorption edges, the discrepancy between models becomes more apparent and our model offers a better description of some experimental results (see discussion in the next section).

#### V. COMPARISON WITH EXPERIMENT

Our model calculation is compared with TEY data obtained in the Brookhaven National Laboratory National Synchrotron Light Source and experiment performed at U15 beamline at (NSLS). The TEY angular profile was obtained by measuring the neutralizing current in a GaAs/AlAs heterostructure versus the grazing angle of incident x rays. The experimental setup has been described elsewhere.<sup>49</sup>

Before we proceed to the discussion of experiment, we would like to consider a radiant energy dissipation pattern in the heterostructure investigated. In Fig. 12 the calculated radiant energy loss is plotted against the incidence angle at different depths in a GaAs overlayer of a GaAs/AlAs heterostructure. One can see that the experimentally measured TEY angular profile, represented by a dashed line, resembles very well the calculated radiant

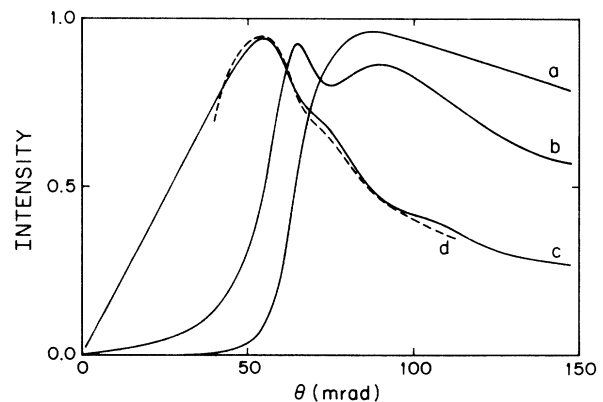


FIG. 12. The calculated normalized radiant energy loss vs incidence angle at different depths in the GaAs overlayer of a GaAs/AlAs heterostructure with a 250-Å overlayer thickness. (a) at depth 248 Å, (b) at depth 125 Å, (c) at depth at 25 Å, (d) TEY obtained from experiment.

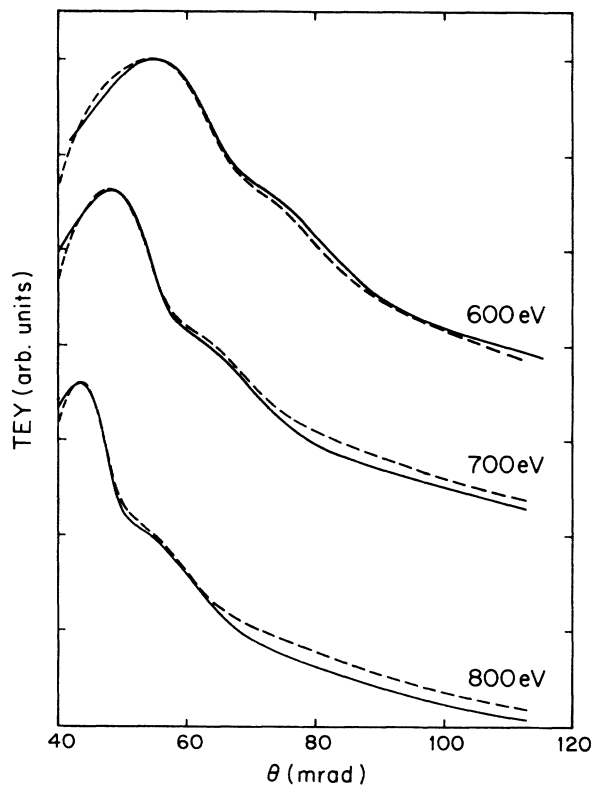


FIG. 13. Comparison of experimental normalized TEY with calculations based on the model proposed in this paper for a GaAs(250 Å)/AlAs heterostructure at 600, 700, and 800 eV of incident photon energy. Solid line, experiment; dashed line, calculations with surface and interface rms roughness equal to 11 and 15 Å, respectively.

losses at the depth of 25 Å. It can be explained by the fact that the IMFP of the average secondary electrons is of the order of tens of Å. This result can be used for an estimation of the attenuation length of the secondaries.

In Fig. 13 the experimental TEY curves are shown with theoretical fits obtained in the framework of the

present model for three different x-ray energies. One can observe characteristic interference oscillations at higher angles due to the presence of the interface, as predicted by the proposed model of TEY. The estimated rms roughness parameters are consistent with those obtained from the total external reflectivity measurements performed on the same heterostructure. The uniform model leads to underestimated values of roughness.<sup>50</sup> This justifies the advantage of our model in this case (i.e., for x-ray energy far away from the absorption edges).

This experiment and previously published results<sup>49,51</sup> obtained for different LSM's demonstrate the usefulness of the TEY method for probing the microstructure of the deep (as compared with secondary-electron IMFP) buried interfaces. One can expect that this method can also be applied for the study of other microstructural parameters, e.g., the concentration of selected atomic species, bulk inhomogeneities, and substrate figure error.

## VI. CONCLUSIONS

In the present paper we discussed the applicability of grazing-incidence total-electron-yield spectroscopy (GATEYS) as a tool for probing the microstructure of layered synthetic materials. We propose a model for describing GATEYS and show that this model agrees well with experiment. We also have demonstrated that the existing model of the uniform TEY production, proposed by Cargill *et al.*,<sup>17,18</sup> is the special case of the present model. We have shown both theoretically and experimentally that the probing depth of GATEYS in LSM is comparable to the characteristic x-ray penetration depth and is not limited by the secondary-electron IMFP. We conclude that GATEYS offers a new tool for microstructure investigations in layered structures.

## ACKNOWLEDGMENTS

The present research is supported by the U.S. Office of Naval Research (ONR) under Grant No. N0001490J1328.

<sup>1</sup>J. Stohr, Jpn. J. Appl. Phys. Supp. **17**, 217 (1978).

<sup>2</sup>P. H. Citrin, P. Eisenberger, and R. C. Hewitt, Phys. Rev. Lett. **45**, 1948 (1980).

<sup>3</sup>D. P. Woodruff, Surf. Int. Anal. **2**, 25 (1988).

<sup>4</sup>G. Martens, P. Rabe, N. Schwentner, and A. Werner, J. Phys. D **11**, 3125 (1978).

<sup>5</sup>G. Martens, P. Rabe, G. Tolken, and A. Werner, Phys. Status Solidi A **55**, 105 (1979).

<sup>6</sup>M. E. Kordesch and R. W. Hoffman, Phys. Rev. B **29**, 491 (1984).

<sup>7</sup>T. Guo and M. L. denBoer, Phys. Rev. B **31**, 6233 (1985).

<sup>8</sup>C. E. Bouldin, R. A. Forman, and M. I. Bell, Phys. Rev. B **35**, 1429 (1987).

<sup>9</sup>W. T. Elam, J. P. Kirkland, R. A. Neiser, and P. D. Wolf, Phys. Rev. B **38**, 26 (1988).

<sup>10</sup>O. Brummer and H. Stephanik, Phys. Status Solidi **36**, 617

(1969).

<sup>11</sup>M. V. Kruglov, V. N. Shchemelev, and G. G. Kareva, Phys. Status Solidi A **46**, 343 (1978).

<sup>12</sup>M. J. Bedzyk, G. Materlik, and M. V. Kovalchuk, Phys. Rev. B **30**, 2453 (1984).

<sup>13</sup>T. Ohta, Y. Kitajima, H. Kuroda, T. Takahashi, and S. Kitakata, Nucl. Instrum. Methods A **246**, 760 (1986).

<sup>14</sup>R. G. Jones and D. P. Woodruff, Surf. Sci. **114**, 38 (1982).

<sup>15</sup>J. Stohr, R. Jaeger, and S. Brennan, Surf. Sci. **117**, 503 (1982).

<sup>16</sup>J. Stohr, C. Nogura, and T. Kendelewicz, Phys. Rev. B **30**, 5571 (1984).

<sup>17</sup>G. S. Cargill III, A. Erbil, R. Frahm, and R. F. Boehme, Bull. Am. Phys. Soc. **32**, 508 (1987).

<sup>18</sup>A. Erbil, G. S. Cargill III, R. Frahm, and R. F. Boehme, Phys. Rev. B **37**, 2450 (1988).

<sup>19</sup>B. L. Henke, J. A. Smith, and D. T. Attwood, J. Appl. Phys.

- 1852 (1977).
- <sup>20</sup>B. L. Henke, J. Liesegang, and S. D. Smith, *Phys. Rev. B* **19**, 3004 (1979).
- <sup>21</sup>A. Krol, C. J. Sher, and Y. H. Kao, *Phys. Rev. B* **38**, 8579 (1988).
- <sup>22</sup>B. Vidal and P. Vincent, *Appl. Opt.* **23**, 1794 (1984).
- <sup>23</sup>K. Feser, *Phys. Rev. Lett.* **28**, 1013 (1972).
- <sup>24</sup>G. Margaritondo and J. H. Weaver, in *Photoemission Spectroscopy of Valence States, Solid State Physics: Surfaces*, edited by R. L. Park and M. G. Lagally (Academic, New York, 1985), Vol. 22, p. 127.
- <sup>25</sup>W. Bambynek, B. Krasemann, R. W. Fink, H. U. Freund, H. Mark, C. D. Swift, R. E. Price, and P. Vanugopala Rao, *Rev. Mod. Phys.* **44**, 716 (1972).
- <sup>26</sup>D. J. Kennedy and S. T. Manson, *Phys. Rev. A* **5**, 227 (1972).
- <sup>27</sup>C. J. Powell, *Surf. Sci.* **44**, 29 (1974).
- <sup>28</sup>R. Shimizu, Y. Kataoka, T. Ikuta, T. Koshikawa, and H. Hashimoto, *J. Phys. D* **9**, 101 (1976).
- <sup>29</sup>L. Reimer, *Scanning Electron Micro.* **2**, 111 (1979).
- <sup>30</sup>M. Inokuti, *Rev. Mod. Phys.* **43**, 297 (1971).
- <sup>31</sup>H. Sugiyama, *Jpn. Bull. Electrotech. Lab.* **38**, 351 (1974).
- <sup>32</sup>C. J. Tung, J. C. Ashley, and R. H. Ritchie, *Surf. Sci.* **81**, 427 (1979).
- <sup>33</sup>J. Szajman and R. C. G. Leckey, *J. Electron Spectros. Relat. Phenom.* **23**, 83 (1981).
- <sup>34</sup>D. R. Penn, *Phys. Rev. B* **35**, 482 (1987).
- <sup>35</sup>J. A. D. Matthew, M. Prutton, M. M. El Gomati, and D. C. Peacock, *Surf. Int. Anal.* **11**, 173 (1988).
- <sup>36</sup>H. Bruining, *Physica* **3**, 1046 (1936).
- <sup>37</sup>H. Salow, *Z. Tech. Phys.* **21**, 8 (1940).
- <sup>38</sup>H. Stolz, *Ann. Phys.* **3**, 197 (1959).
- <sup>39</sup>K. Kanaya and S. Okayama, *J. Phys. D* **5**, 43 (1972).
- <sup>40</sup>T. Koshikawa and R. Shimizu, *J. Phys. D* **7**, 1303 (1974).
- <sup>41</sup>J. J. Quinn, *Phys. Rev.* **126**, 1453 (1962).
- <sup>42</sup>H. W. Streitwolf, *Ann. Phys.* **3**, 183 (1959).
- <sup>43</sup>H. Seiler, *Z. Angew. Phys.* **3**, 249 (1967).
- <sup>44</sup>H. Kanter, *Phys. Rev. B* **1**, 522 (1969).
- <sup>45</sup>I. Lindau and W. E. Spicer, *J. Electron Spectros. Relat. Phenom.* **3**, 409 (1974).
- <sup>46</sup>M. P. Seah and W. A. Dench, *Surf. Int. Anal.* **1**, 2 (1979).
- <sup>47</sup>J. Szajman, J. Liesegang, J. G. Jenkin, and R. C. G. Leckey, *J. Electron Spectros. Relat. Phenom.* **23**, 97 (1981).
- <sup>48</sup>J. C. Ashley and V. E. Anderson, *J. Electron Spectros. Relat. Phenom.* **24**, 127 (1981).
- <sup>49</sup>A. Krol, C. J. Sher, D. R. Storch, S. C. Woronick, L. Krebs, Y. H. Kao, and L. L. Chang, *Mater. Res. Soc. Symp. Proc.* **143**, 25 (1989).
- <sup>50</sup>A. Krol, C. J. Sher, H. Resat, S. C. Woronick, W. Ng, Y. H. Kao, L. L. Chang, and J. M. Hong, *Mater. Res. Soc. Symp. Proc.* **103**, 335 (1988).
- <sup>51</sup>A. Krol, C. J. Sher, D. R. Storch, S. C. Woronick, L. Krebs, Y. H. Kao, L. L. Chang, and H. Munekata, *Surf. Sci.* **228**, 108 (1990).